Anisotropy in mechanical properties of 3D-printed layered concrete

G.S. Slavcheva ✉ (iD) , **A.V. Levchenko** (iD) , **M.A. Shvedova** (iD) , **D.R. Karakchi-ogly**, **D.S. Babenko**

Voronezh State Technical University, Voronezh, Russian Federation

✉ *gslavcheva@yandex.ru*

Keywords: additive manufacturing, 3D-printed concrete, mechanical properties, strength, anisotropy

Abstract. The article presents the results of studying the mechanical properties of 3D-printed layered concrete (3DPLC), including compressive, flexural, and splitting strength. To assess them, we used a compression test with a load applied perpendicular and parallel to the printed direction; a flexural test with a load applied perpendicular to the printed direction, and a splitting test to evaluate the interlayer bond strength upon the transfer of force along the boundary surface parallel to the printing direction. The mechanical properties of reference cast concrete (CC) were evaluated in accordance with the requirements of Russian standards. We established a significant anisotropy of the mechanical properties of 3DPLC along and perpendicular to the printed layers as well as a significant reduction in all strength values compared to similar values of reference CC. The printing time gap was the determining factor in the reduction of values of the mechanical properties for 3DPLC. When it increased to 20 minutes, a critical decrease in the interlayer bond strength was observed. At the same time, a threefold drop in the strength of 3DPLC compared to similar characteristics of CC could be observed in case of a decrease in humidity and a change in temperature in the range of +(10–30) °C. The impact of the curing condition on the variability of the mechanical properties of 3DPLC depended on the particle size distribution of fillers and aggregates that determined the surface roughness of the printed layer. The range of changes in the strength of sand-based printed concrete in case of varying temperature and humidity of curing (with a similar printing time gap) was 30–70 %, and for limestone-based printed concrete it was 1.5–3 times.

1. Introduction

Realizing the potential of 3D-build printing is associated not only with the possibilities of robotic construction of buildings, but also with the issues of calculation and design of hollow 3D-printed structures. Therefore, it is highly important to adequately evaluate the strength properties and standardize the classes of 3D-printed layered concrete (3DPLC).

Unlike traditional mold cast concrete (CC), strongly pronounced anisotropy of mechanical properties is typical for 3DPLC. Depending on the printing technology, constructions may have 2 types of stratification. Layering the next layer on top of the previous one creates horizontal stratification. If the next layer is layered next to the previous one on the same level, it may result in vertical and horizontal stratification. The strength

of a single-layer material $\left(R_{cc}\right)$ is greater than the strength of 3DPLC on the whole. However, upon the load action, the strength along the layers $\left(R_x\right)$ and across the layers $\left(R_y\right)$ significantly decreases.

The anisotropy in mechanical properties of 3DPLC is an object of present research.

In their review, A.U. Rehman and J.H. Kim [1] summarized and compared data from dozens of previous studies that presented relationships between the strength of 3DPLC along the layers $\left(R_x\right)$ and across the layers $\left(R_y\right)$ and the strength of the layer material $\left(R_{cc}\right)$. According to the results of different studies, these ratios varied greatly in the following range:

- compressive strength $R_{cx}/R_{cc} = 0.5-1.1,\ R_{cy}/R_{cc} = 0.6-1.1;$

- flexural strength $R_{fx}/R_{fc} = 0.3-0.9,\ R_{fy}/R_{fc} = 0.9-1.3;$

- tensile strength $R_{tx}/R_{tc} = 0.8-1.5,\ R_{ty}/R_{tc} = 0.3-0.5.$

It is obvious that the strength of 3DPLC is determined by the interlayer bond at the vertical and horizontal boundaries of layer separation. However, many studies [2–16] show that the strength of 3DPLC, compared to CC, decreased directly proportional to the printing time gap. In [3, 5, 7] it was shown that the strength and nature of destruction of layered printed samples was similar to the presented parameters of mold cast samples when layered with a printing time gap of up to 5 min. As the time interval between layering increased, the nature of the destruction changed, and cracks passed through the surface of the layer bond. Therefore, differences in the mechanical behavior of printed and cast concrete could be determined by interlayer effects that influence the path of crack development and failure patterns. As a result, the bond strength between the layers as well as compressive, flexural, and splitting strength of 3DPLC decreased. The interval of 20–30 minutes is considered critical, and exceeding this limit leads to self-destruction of the samples.

However, a more detailed analysis of the conditions of the experiments carried out in [2–15], the data of which were summarized and compared in [1], showed that in all cases the printing time gap did not exceed 1 minute [3, 8–14]. Therefore, the variability described above in data from different studies on the ratio of strength of 3DPLC and CC cannot be classified as the effect of this factor alone. In the analyzed research data, the compositions of mixtures varied significantly in their appearance and particle size distribution of fine aggregates and fillers [4, 9, 11–14] as well as printed samples curing. A number of works [16–19] used mixtures based on sand without fillers, while in [2, 20–21] they used mixtures that included various fillers (fly ash, silica fume, etc.) apart from fine aggregates. After printing, the curing state of samples also varied among different studies, mainly in the humidity of curing, which varied in the range of RH = 60–100 % [2, 13–16].

Based on this, it can be assumed that the interlayer bond strength and, correspondingly, mechanical properties of 3DPLC, apart from printing time gap, are determined by the following factors.

1. Temperature and humidity of curing. Interlayer bond strength of 3D-printed materials significantly depends on the open time, the time during which technological characteristics of fresh 3D-printable mixture (viscosity, plasticity) are preserved unchanged. In the works of A. Perrot et al. [22–24], it was proved that a decrease in the interlayer bond strength depended on the structural build-up rate: the greater the rate of curing was, the more impact the time between layering had on strength. This was due to the fact that temperature and humidity significantly affect the hydration and curing speed of cement paste.

2. Roughness of the layer surface depended on the particle size distribution of fillers and aggregates in the mixture. The roughness of the layer surface influenced the energy and the number of bonds at the interface between the layers, and therefore it can greatly affect the formation of the mechanical properties of 3DPLC.

The influence of these factors on the strength of 3DPLC has not been investigated, which determines the relevance of the research. The results presented here may have implications for use in the design of 3D-printed structure.

As a consequence, the present research aims to investigate the mechanical behavior and anisotropy properties of 3DPLC. In particular, the effects of three parameters on the properties of 3DPLC are considered as the objectives of present research:

  – printing time gap;
  – curing conditions – temperature and humidity;
  – particle size distribution of fillers and aggregates used in mixtures.

2. Materials and methods

The studies were performed on two types of 3D-printable mixtures, the compositions of which were optimized by the authors in previous studies regarding extrudability, buildability, and strength of the layer material (Table 1):

1. sand-based mixture, patent RU 2729085 C1 [25];

2. limestone-based mixture, patent RU 2729283 C1 [26].

The initial components were used in the mixtures:
  – Portland cement CEM I 42.5 R (EN 197-1:2011);
  – Sika® plasticizer based on polycarboxylate ether;
  – viscosity modifying admixture – metakaolin ($Al_2O_3 \cdot SiO_2$ content ~ 98 %, particle size distribution ranging from 1 to 5 μm);
  – polypropylene fiber (l = 12 mm, d = 0.022–0.034 mm);
  – limestone filler ($CaCO_3$ content ~ 95 %; particle size distribution ranging from 10 to 75 μm), silica sand (SiO_2 content ~ 95 %; particle size distribution ranging from 160 to 1200 μm).

Table 1. Concrete mixture design.

Mixture type	Components / mass cement (%)					W/C
	Plasticizer	Metakaolin	Polypropylene fiber	Silica sand	Limestone filler	
Sand-based	1.2	2	0.5	125	–	0.29
Limestone-based	1.2	2	0.5	–	100	0.39

To study and evaluate the mechanical properties of 3DPLC, an element ~ 50 cm long, 4 cm wide, and 16 cm high was printed on laboratory printer. The cross section of the layer was 40 × 20 mm, and the number of printed layers was 8. The following printing modes were used during the studies:

  – constant print speed 20 mm/sec;
  – constant distance between the nozzle and the layer 20 mm;
  – variable printing time gap Δt = 0.5 min, 10 min, 30 min;

After printing, the 3D-printed samples were stored for 28 days in a different environment:

  – standardized (T = 20 ± 2 °C, RH = 100 % (reference));
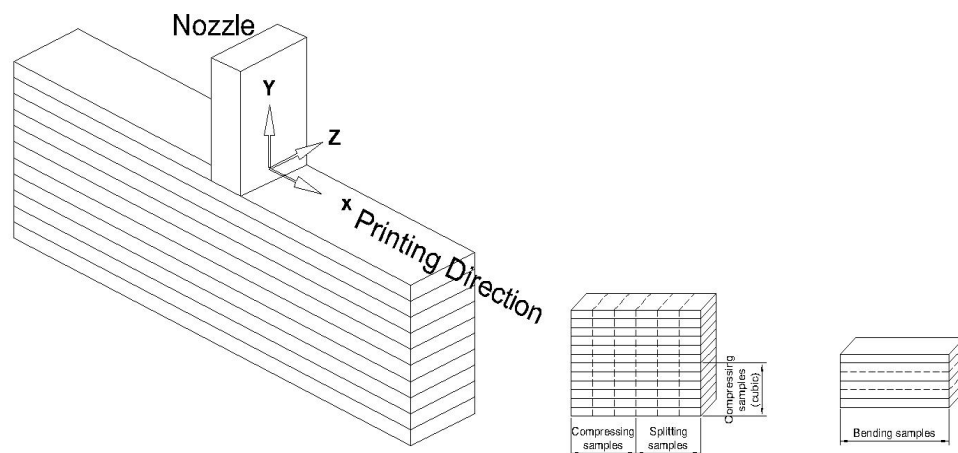 – modelling (T = 10 ± 2 °C, RH = 60 %, T = 20 ± 2 °C, RH = 60 %, T = 30 ± 2 °C, RH = 60 %).

Figure 1. Scheme for preparing 3DPLC-sample for strength tests.

After curing, the model element was sawn into prism samples with the size of 40 × 40 × 160 mm.

The cutting layout of a 3D-printed model element is presented in Fig. 1.

Mechanical properties of CC were assessed as reference ones. In order to do this, reference mold samples were made from each batch of sand-based and limestone-based mixtures during the research simultaneously with the printing of model fragments. The mold samples were stored for 28 days in a standardized environment (T = 20 ± 2 °C, RH = 100 %).

3DPLC samples were tested as follows:

- compression test upon load application across the printed direction (Y-axes) – 3 prism samples in a series;
- compression test upon load application along the printed direction (X-axes) – 6 half-prism samples in a series;
- flexural test upon load application across the printed direction (Y-axes) – 3 prism samples in a series;
- splitting test to assess the interlayer bond strength with point force along the boundary surface in the sample along the printed direction (X-axes) – 3 prism samples in a series.

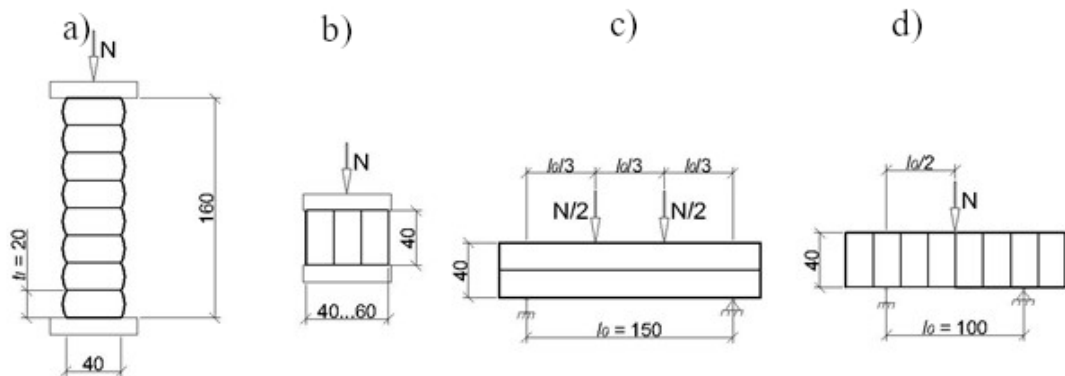Test patterns for 3DPLC samples are presented in Fig. 2.

Figure 2. Schemes for strength testing of 3DPLC-samples: (a) compressive strength test (Y-axes); (b) compressive strength test (X-axes); (c) four-point bending test (Y-axes); (d) splitting three-point bending test (X-axes).

The mold CC samples were tested according to Russian State Standard GOST 10180 "Concretes. Methods for strength determination using reference specimens".

A summary of the tests is presented in Table 2. Each set of sample is indicated by an abbreviation, where:

- CC is for the cast concrete;
- PLC is for the 3D-printed layered concrete;
- LM is for the limestone-based mixture;
- S is for the sand-based mixture.

Table 2. Test matrix.

Variables	Abbreviation			
	CC-S	CC-LM	PLC-S	PLC-LM
Printing Time Gap (min)	No	No	0, 10, 20	0, 10, 20
Samples curing (T; RH)	20 °C, 100 %	20 °C, 100 %	20 °C, 100 %; 20 °C, 60 %; 10 °C, 60 %; 30 °C, 60 %;	20 °C, 100 %; 20 °C, 60 %; 10 °C, 60 %; 30 °C, 60 %;
Load direction of compression test	According to Russian State Standard GOST 10180-2012 "Concretes. Methods for strength determination using reference specimens"		Y-axes, X-axes	Y-axes, X-axes
Load direction of flexural test			Y-axes	Y-axes
Load direction of splitting test			X-axes	X-axes

After mechanical tests were conducted, the destruction surface of the samples was examined on a desktop scanning electron microscope Thermo Scientific™ Phenom™ XL. We used the Phenom Desktop SEM software to operate the microscope as well as to obtain, process, and analyze the images. This software includes the Element Identification program, which can be used to operate the built-in EMF detector and to work with the information received from it.

3.   Results and Discussion

According to the test results, we recorded a change in all mechanical properties of 3DPLC, compared to similar values of CC (Tables 3–5). The changes in the samples that were stored in a standardized environment were the following:

- prismatic strength upon axial compression and load application across the printed direction (Y-axes) decreased by 1.8 and 2.4 times for sand-based and limestone-based printed concrete, respectively;
- axial compressive strength upon load application along the printed direction (X-axes) reduced by 1.15 and 1.4 times for sand-based and limestone-based printed concrete, respectively;
- the strength at four-point load application across the printed direction (Y-axes), on the contrary, increased by 1.8 times for sand-based and limestone-based printed concrete;
- interlayer bond strength, according to splitting test, upon load application along the printed direction (X-axes) decreased by 2.1 and 1.4 times for sand-based and limestone-based printed concrete, respectively.

It is highly important that a significant anisotropy of 3DPLC properties was established. The compressive strength upon loading along and across the printed direction differed by 2–2.1 times, while the bending strength differed by 2.5–3.6 times. The loading conditions have the most significant influence on the level of anisotropy. The nature of the uniaxial compressive strength – displacement curves (Fig. 3, 4) for 3DPLC and CC differed most significantly in the tests with a load application along the printed direction (X-axes). A decrease in the slope of the ascending branch and the appearance of a long descending branch on the deformation curves are typical for 3DPLC-samples. Thus, the mechanical behavior of 3DPLC is characterized by the emergence of pseudo-plastic deformations.

Table 3. CC mechanical properties.

Mechanical properties	Mixture type	
	Sand-based	Limestone-based
Uniaxial compressive strength (prism) R_y^cc, MPa	49.33	46.98
Uniaxial compressive strength (cube) R_x^cc, MPa	3.90	2.80
Flexural strength $R_\mathrm{fy}^\mathrm{cc}$, MPa (according to four-point bending test)	3.90	2.80
Splitting strength $R_\mathrm{sx}^\mathrm{cc}$, MPa	4.04	2.97

Table 4. Sand-based 3DPLC mechanical properties.

Mechanical properties	Temperature and humidity of curing			
	T = 20 ± 2 °C, RH = 100 %	T = 10 ± 2 °C, RH = 60 %	T = 20 ± 2 °C, RH = 60 %	T = 30 ± 2 °C, RH = 60 %
Printing time gap Δt = 0.5 min				
Uniaxial compressive strength (Y-axes) R_y, MPa	27.65	19.48	24.89	16.27
Flexural strength (Y-axes) R_fy, MPa	6.92	5.70	6.46	6.48
Uniaxial compressive strength (X-axes) R_x, MPa	54.69	45.02	49.66	41.88

Mechanical properties	Temperature and humidity of curing			
	T = 20 ± 2 °C, RH = 100 %	T = 10 ± 2 °C, RH = 60 %	T = 20 ± 2 °C, RH = 60 %	T = 30 ± 2 °C, RH = 60 %
Interlayer bond (according to splitting test (X-axes)) R_{sx}, MPa	1.94	1.78	1.92	1.48
Printing time gap Δt = 10 min				
Uniaxial compressive strength (Y-axes) R_y, MPa	–	19.28	22.39	21.35
Flexural strength (Y-axes) R_{fy}, MPa	–	4.62	4.97	4.86
Uniaxial compressive strength (X-axes) R_x, MPa	–	49.87	51.26	45.07
Interlayer bond (according to splitting test (X-axes)) R_{sx}, MPa	–	0,82	1.53	1.57
Printing time gap Δt = 20 min				
Uniaxial compressive strength (Y-axes) R_y, MPa	–	–	–	–
Flexural strength (Y-axes) R_{fy}, MPa	–	3.10	3.60	3.89
Uniaxial compressive strength (X-axes) R_x, MPa	–	36.89	33.61	31.56
Interlayer bond (according to splitting test (X-axes)) R_{sx}, MPa	–	0.32	0.76	1.01

Table 5. Limestone-based 3DPLC mechanical properties.

Mechanical properties	Temperature and humidity of curing			
	T = 20±2 °C, RH = 100 %	T = 10±2 °C, RH = 60 %	T = 20±2 °C, RH = 60 %	T = 30±2 °C, RH = 60 %
Printing time gap Δt = 0.5 min				
Uniaxial compressive strength (Y-axes) R_y, MPa	19.76	11.20	19.34	14.74
Flexural strength (Y-axes) R_{fy}, MPa	5.10	3.88	6.10	6.45
Uniaxial compressive strength (X-axes) R_x, MPa	41.91	37.99	41.13	36.51
Interlayer bond (according to splitting test (X-axes)) R_{sx}, MPa	2.08	0.67	2.55	2.27
Printing time gap Δt = 10 min				
Uniaxial compressive strength (Y-axes) R_y, MPa	–	–	15.89	–
Flexural strength (Y-axes) R_{fy}, MPa	–	3.95	4.74	5.52
Uniaxial compressive strength (X-axes) R_x, MPa	–	32.36	41.15	31.93
Interlayer bond (according to splitting test (X-axes)) R_{sx}, MPa	–	0.39	0.94	0.94

a)

b)

**Figure 3. Uniaxial compressive strength – displacement curves
(load across the printed direction (Y-axes)): (a) sand-based concrete;
(b) limestone-based concrete.**

Regarding the impact of technological parameters varied in experiments on the mechanical properties of 3DPLC, we established the following.
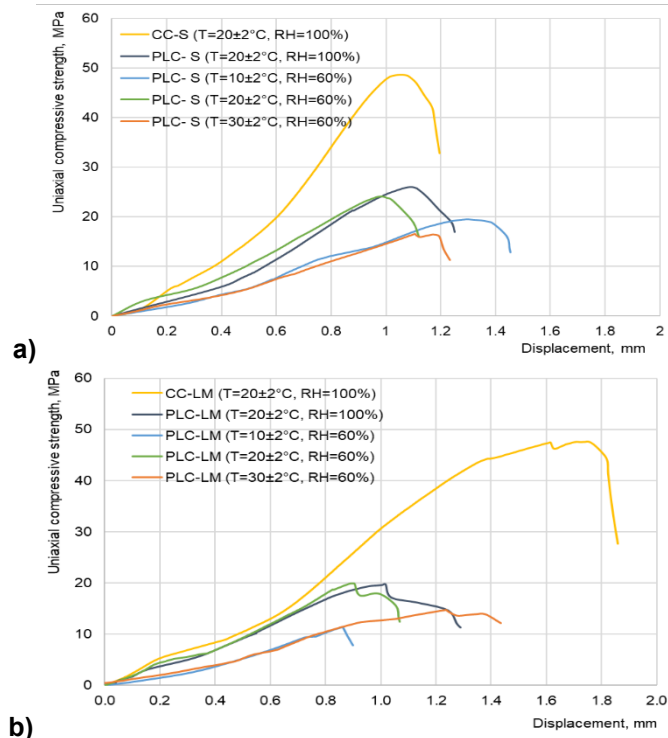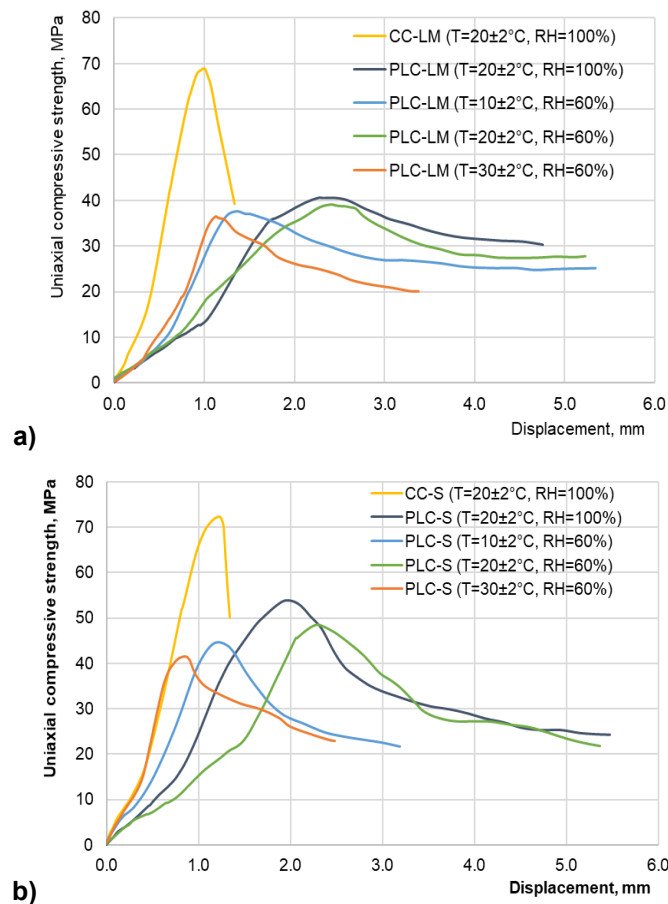

a)

b)

**Figure 4. Uniaxial compressive strength – displacement curves
(load along the printed direction (X-axes)): (a) sand-based concrete;
(b) limestone-based concrete.**

Printing time gap. Uniaxial compressive strength of 3DPLC (upon load application across the printed direction (Y-axes)), compared to CC, decreased by 1.8–3.0 times and by 2.3–4.2 times for sand-based and limestone-based printed concrete, respectively (Tables 1–3). As for the samples printed with the printing time gap Δt = 0.5 min and Δt = 10 min, the strength values with similar temperature and humidity conditions differed by less than 10–15 %. The samples printed with the Δt = 20 min split along the layer in the course of sawing, and the values of prismatic strength could not be recorded. Upon load application along the printed direction (X-axes), the compressive strength of 3DPLC decreased less significantly, compared to the compressive strength of CC. The decrease was by 1.15–1.5 times with Δt = 0.5 min and Δt = 10 min, while with Δt = 20 min it decreased by 1.7–2.0 times depending on temperature and humidity conditions of curing.

On the contrary, flexural strength of layered samples (upon a four-point bend and load application across the printed direction (Y-axes)), compared to CC, decreased by 1.2–1.8 times and by 1.4–2.3 times for sand-based and limestone-based printed concrete, respectively. The greatest increase of strength was observed for the samples with Δt = 0.5 min, which was by 1.5–2.3 times depending on temperature and humidity conditions of curing. An increase of strength for the samples with Δt = 10 min was by 1.2–1.3 times, and with Δt = 20 min the strength of 3DPLC samples was similar to its values for CC samples.

Interlayer bond strength of 3DPLC-samples, according to the splitting test (load direction along the printed direction (X-axes)), compared to the strength of CC samples with Δt = 0.5 min, decreased by 2.1–2.7 times, with Δt = 10 min – by 2.5–4.9 times, with Δt = 20 min – by 4–12 times depending on temperature and humidity conditions of curing. The samples printed with Δt = 10 min under all temperature and humidity conditions of curing had the interlayer bond strength of less than 1 MPa. The interlayer bond strength significantly decreased with Δt = 20 min, which was also confirmed by the destruction of layered samples in the course of cutting into prisms.

Temperature and humidity of curing. The humidity conditions of curing have the greatest impact on the change in strength for the entire set of mechanical properties, in all the studied cases of the time interval between the layering of layers. For all mechanical properties of 3DPLC cured at RH = 60 % and T = (10 – 30) ± 2 °C a decrease by 1.1–1.7 times was typical compared to similar samples cured under normal conditions (T = 20 ± 2 °C, RH = 100 %). The prismatic strength of the samples (Δt = 0.5 min) decreased most significantly upon curing RH = 60 % and T = 30±2 °C, by 1.7–1.8 times. Mechanical properties of 3DPLC cured at T = 10 ± 2 °C, RH = 60 %, and T = 30 ± 2 °C, RH = 60 %, were usually 10–35 % lower than the similar characteristics of the samples cured at T = 20 ± 2 °C, RH = 60 %.

With an increase in the printing time gap, the strength of limestone-based concrete decreased more, compared to sand-based concrete. At the same time, the variability of all strength characteristics of limestone-based concrete with varying temperature and humidity of curing was also higher.

According to the obtained experimental data, the range of variability of the ratios between the strength of 3DPLC along the layers $\left(R_{\mathrm{y}} \right)$ and across the layers $\left(R_{\mathrm{x}} \right)$ and the strength of the layer material $\left(R^{\mathrm{cc}} \right)$ was as follows (Fig. 5):

– compressive strength $R_{\mathrm{y}}/R_{\mathrm{y}}^{\mathrm{cc}}=0.24-0.56$; $R_{\mathrm{x}}/R_{\mathrm{x}}^{\mathrm{cc}}=0.51-0.87$,

– flexural strength $R_{\mathrm{fy}}/R_{\mathrm{fy}}^{\mathrm{cc}}=1.18-1.97$,

– splitting strength $R_{\mathrm{sx}}/R_{\mathrm{sx}}^{\mathrm{cc}}=0.13-0.86$.

The change in the mechanical properties of 3DPLC, compared to CC, was mainly determined by the specific aspects of the destruction of the layered structure upon the load action.

In case of axial compression (upon load application across the printed direction (Y-axes)), the destruction was characterized by the development of vertical cracks that crossed the layers with no changes in their crack path (Fig. 6a). Therefore, a significant decrease in the Y-axes compressive strength of 3DPLC, compared to the strength of CC, can be explained by weakening of material structure due to its layering. According to electron microscopy analysis, microdefects up to 100 μm were recorded at the boundary between the layers, which, upon load action, served as stress concentrators and contributed to the formation and development of cracks along the boundary line as well as across the layers (Fig. 7a).

The decrease in the X-axes compressive strength of 3DPLC, compared to CC, was less significant. In this case, when upon axial compression the load action was along the layers, the destruction was characterized by the development of multiple vertical cracks along the boundary surfaces as well as in the body of a single layer (Fig. 6b). This was associated with the fact that in this case of loading, the material of the layer makes a more significant contribution to the destruction resistance, which reduces the negative effect of weakening the material structure due to its layering.

In case of four-point bending, the load is applied across the layers (Y-axes), and the destruction is characterized by the development of a vertical crack that changes its path at the boundary surface (Fig. 6c) of 3DPLC-samples. Therefore, an increase in the flexural strength of 3DPLC, compared to the strength of CC, was due to the damping effect of the crack at the boundary surface.

When splitting, destruction occurs along the boundary of the adhesive bond between the layers (Fig. 6d), therefore, the roughness of the layer surface naturally affected the interlayer bond strength. According to SEM data, the destruction surface at the boundary surface for limestone-based concrete was smoother and more homogeneous (Fig. 7b), while for sand-based concrete (Fig. 7c) it was rougher due to the presence of sand grains. As a result, the decrease of splitting strength 3DPLC, compared to CC, was more significant for limestone-based concrete than for sand-based concrete.

Based on the obtained experimental data, it can be stated that the printing time gap was the determining factor in the reduction of values of the mechanical properties for 3DPLC. When it was increased to 20 minutes, we observed a critical reduction in the interlayer bond strength, which led to significant decrease in the values of all mechanical properties of 3DPLC, up to the self-destruction of the samples. This is in full agreement with the data of other researchers in [3, 5, 7, 8].

The novelty of the obtained results is that we clearly established a significant influence of the curing condition (temperature and humidity) on the variability level of the ratio between the mechanical properties of 3DPLC and CC $\left(R^{\mathrm{3DPLC}}/R^{\mathrm{CC}} \right)$. The $R^{\mathrm{3DPLC}}/R^{\mathrm{CC}}$ ratio can decrease by up to 3 times in case of changes in temperature and humidity of curing.
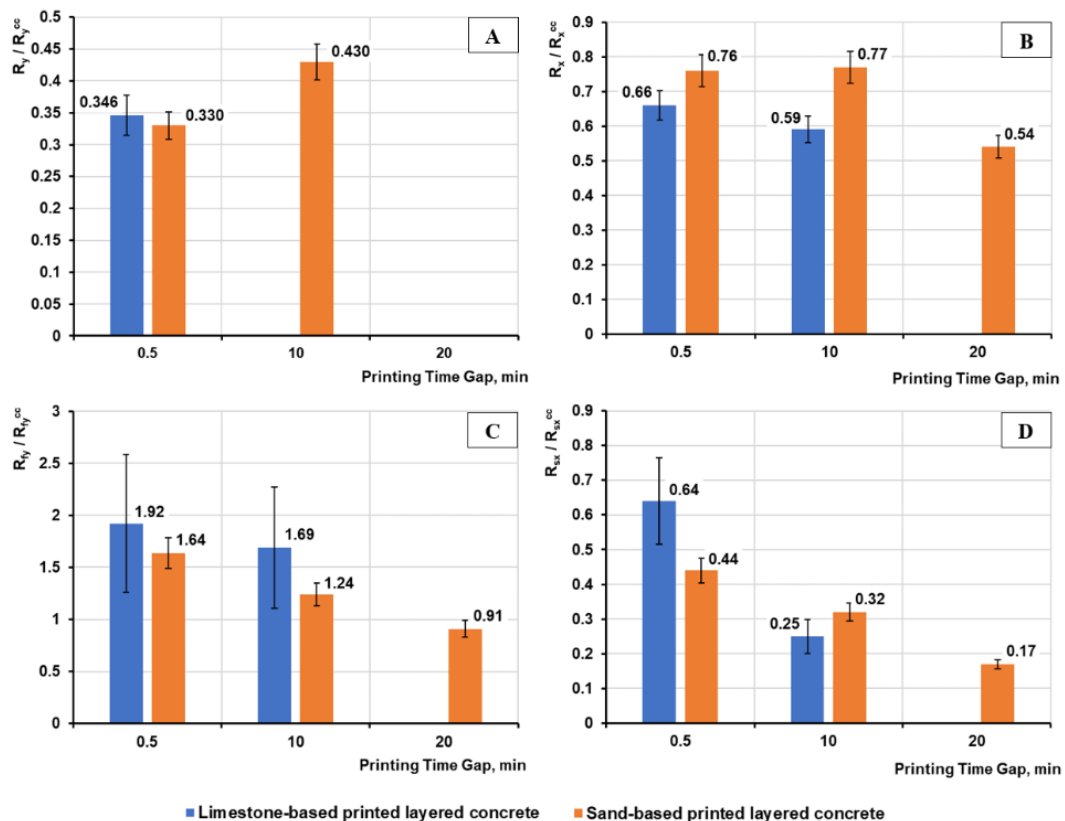

Figure 5. Anisotropy in mechanical properties of 3DPLC:
(a) uniaxial compressive strength (Y-axes); (b) uniaxial compressive strength (X-axes);
(c) flexural strength (Y-axes); (d) interlayer bond (according to splitting test (X-axes).
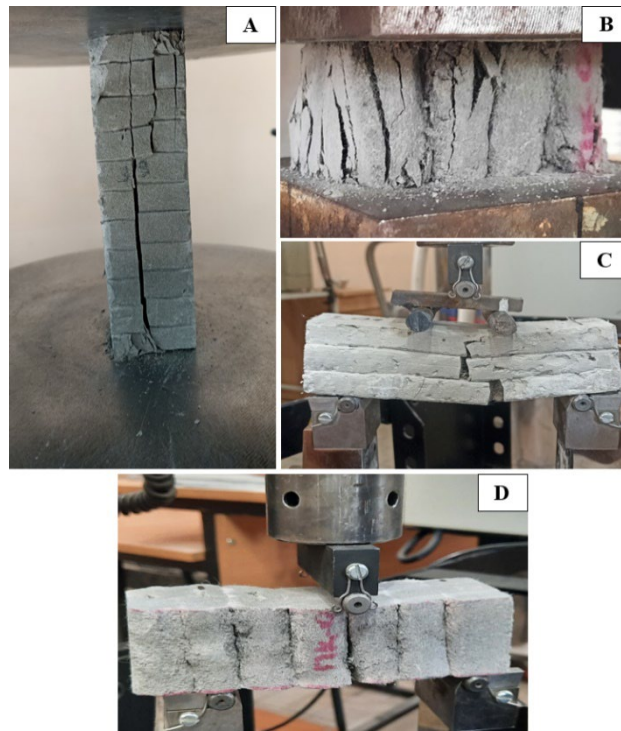
**Figure 6. Strength tests of 3DPLC-samples: (a) uniaxial compressive test (Y-axes);
(b) uniaxial compressive test (X-axes); (c) four-point bending test (Y-axes);
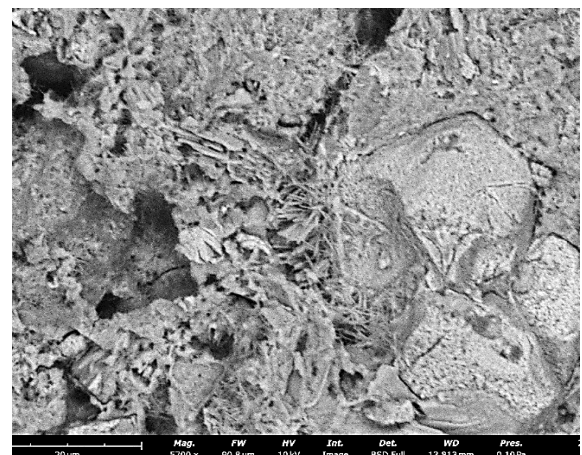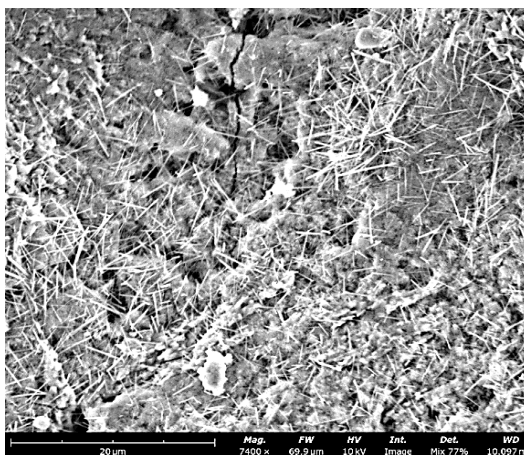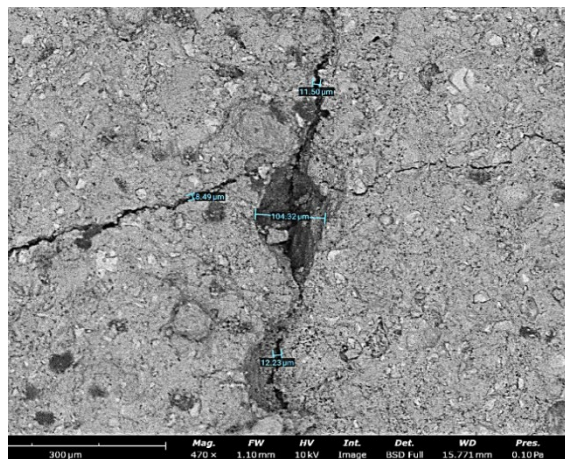(d) splitting three-point bending test (X-axes).**

**Figure 7. Micrographs of the fracture surface for 3DPLC: (a) across the printed layer;
(b) along the printed layer for limestone-based concrete; (c) along the printed layer
for sand-based concrete.**

The effect of a decrease in strength in case of reduction in temperature and humidity of curing was logically associated with a slowdown in the processes of cement hydration and corresponding decrease in the strength of the layer material. On the contrary, decrease in strength of 3DPLC related to the increasing temperature can be associated with increased setting rate and a corresponding decrease in the adhesion strength of the layers.

The extent to which curing condition influenced the variability of the mechanical properties of 3DPLC depended on the particle size distribution of fillers and aggregates. The range of changes in the mechanical properties of sand-based 3DPLC in case of varying temperature and humidity of curing (with printing time gap Δt = const) was 30–70 %, and for limestone-based 3DPLC it was 1.5–3 times. As noted above, this is explained by the factor of the layer surface roughness. When the hydration and curing conditions changed, the mechanical interlocking forces contributed more to the provision of interlayer bond strength, which could partially compensate for the physicochemical interactions at the boundary surface.

In conclusion, it is important to emphasize that at this stage of research we have not identified any clear quantitative patterns of the effect of temperature and humidity on certain types of strength values. The research must be expanded in order to obtain them.

4. Conclusions

1. A significant anisotropy of mechanical properties of 3D-printed layered concrete (3DPLC) along $\left(R_{\mathrm{x}}\right)$ and across $\left(R_{\mathrm{y}}\right)$ the printed layers was established. At the same time, a decrease in all values of strength with similar values of mold cast concrete (CC) was typical for 3DPLC. The range of variation in the ratio between the strength of 3DPLC and CC depended on the direction of load application regarding the direction of printing layers and was as follows:

   – compressive strength $R_{\mathrm{y}}\big/R_{\mathrm{y}}^{\mathrm{cc}} = 0.24 - 0.56;\ \ R_{\mathrm{x}}\big/R_{\mathrm{x}}^{\mathrm{cc}} = 0.51 - 0.87;$

   – flexural strength $R_{\mathrm{fy}}\big/R_{\mathrm{fy}}^{\mathrm{cc}} = 1.18 - 1.97;$

   – splitting strength $R_{\mathrm{sx}}\big/R_{\mathrm{sx}}^{\mathrm{cc}} = 0.13 - 0.86.$

2. The printing time gap was the determining factor in the reduction of values of the mechanical properties for 3DPLC. When it was increased to 20 min, we observed a critical reduction in the interlayer bond strength, which led to significant decrease in values of all mechanical properties of 3DPLC, up to self-destruction of the samples.

3. We established a significant influence of the curing condition (temperature and humidity) on the variability level of the ratio between the strength of 3DPLC and CC $\left(R^{\mathrm{3DPLC}}\big/R^{\mathrm{CC}}\right)$. A threefold drop in the strength of 3DPLC, compared to similar characteristics of CC, could be observed in case of a decrease in humidity and a change in temperature in the range of + (10–30) °C.

4. The impact of the curing condition on the variability of the mechanical properties of 3DPLC depended on the particle size distribution of fillers and aggregates that determined the surface roughness of the printed layer. The range of changes in the strength of 3DPLC in case of varying temperature and humidity of curing (with printing time gap Δt = const) was 30–70 %, and for limestone-based 3DPLC it was 1.5–3 times.

References

1. Rehman, A.U., Kim, J.H. 3D concrete printing: A systematic review of rheology, mix designs, mechanical, microstructural, and durability characteristics. Materials. 2021. 14 (14). 3800. DOI: 10.3390/ma14143800

2. Le, T.T., Austin, S.A., Lim, S., Buswell, R.A., Law, R., Gibb, A.G.F., Thorpe, T. Hardened properties of high-performance printing concrete. Cement and Concrete Research. 2012. 42 (3). Pp. 558–566. DOI: 10.1016/j.cemconres.2011.12.003

3. Panda, B., Mohamed, N.A.N., Paul, S.C., Singh, G.V.P.B., Tan, M.J., Šavija, B. The effect of material fresh properties and process parameters on buildability and interlayer adhesion of 3D printed concrete. Materials. 2019. 12 (13). 2149. DOI: 10.3390/ma12132149

4. Wang, L., Jiang, H., Li, Z., Ma, G. Mechanical behaviors of 3D printed lightweight concrete structure with hollow section. Archives of Civil and Mechanical Engineering. 2020. 20. 16. DOI: 10.1007/s43452-020-00017-1

5. Chen, Y., Jansen, K., Zhang, H., Romero Rodriguez, C., Gan, Y., Çopuroğlu, O., Schlangen, E. Effect of printing parameters on interlayer bond strength of 3D printed limestone-calcined clay-based cementitious materials: An experimental and numerical study. Construction and Building Materials. 2020. 262. 120094. DOI: 10.1016/j.conbuildmat.2020.120094

6. Marchment, T., Sanjayan, J., Xia, M. Method of enhancing interlayer bond strength in construction scale 3D printing with mortar by effective bond area amplification. Materials & Design. 2019. 169. 107684. DOI: 10.1016/j.matdes.2019.107684

7. Keita, E., Bessaies-Bey, H., Zuo, W., Belin, P., Roussel, N. Weak bond strength between successive layers in extrusion-based additive manufacturing: measurement and physical origin. Cement and Concrete Research. 2019. 123. 105787. DOI: 10.1016/j.cemconres.2019.105787

8. Zareiyan, B. Khoshnevis, B. Effects of interlocking on interlayer adhesion and strength of structures in 3D printing of concrete. Automation in Construction. 2017. 83. Pp. 212–221. DOI: 10.1016/j.autcon.2017.08.019

9. Ducoulombier, N., Demont, L., Chateau, C., Bornert, M., Caron, J.F. Additive manufacturing of anisotropic concrete: A flow-based pultrusion of continuous fibers in a cementitious matrix. Procedia Manufacturing. 2020. 47. Pp. 1070–1077. DOI: 10.1016/j.promfg.2020.04.117

10. Karpova, E., Skripkiunas, G., Sedova, A., Tsimbalyuk, Y. Additive manufacturing of concrete wall structures. Proceedings of IV International Scientific Conference "Construction and Architecture: Theory and Practice of Innovative Development" (CATPID-2021 Part 1). Nalchik, 2021. DOI: 10.1051/e3sconf/202128103007

11. Dielemans, G., Briels, D., Jaugstetter, F., Henke, K., Dörfler, K. Additive Manufacturing of Thermally Enhanced Lightweight Concrete Wall Elements with Closed Cellular Structures. Journal of Facade Design and Engineering. 2021. 9 (1). Pp. 59–72. DOI: 10.7480/jfde.2021.1.5418

12. Zhu, B., Pan, J., Nematollahi, B., Zhou, Z., Zhang, Y., Sanjayan, J. Development of 3D printable engineered cementitious composites with ultra-high tensile ductility for digital construction. Materials & Design. 2019.181. 108088. DOI: 10.1016/j.matdes.2019.108088

13. Panda, B., Paul, S.C., Mohamed, N.A.N., Tay, Y.W.D., Tan, M.J. Measurement of tensile bond strength of 3D printed geopolymer mortar. Measurement. 2018. 113. Pp. 108–116. DOI: 10.1016/j.measurement.2017.08.051

14. Classen, M., Ungermann, J., Sharma, R. Additive manufacturing of reinforced concrete-development of a 3D printing technology for cementitious composites with metallic reinforcement. Applied Sciences. 2020. 10 (11). 3791. DOI: 10.3390/app10113791

15. Katzer, J., Szatkiewicz, T. Properties of concrete elements with 3D printed formworks which substitute steel reinforcement. Construction and Building Materials. 2019. 210. Pp. 157–161. DOI: 10.1016/j.conbuildmat.2019.03.204

16. Ji, G., Ding, T., Xiao, J., Du, S., Li, J., Duan, Z. A 3D printed ready-mixed concrete power distribution substation: Materials and construction technology. Materials. 2019. 12 (9). 1540. DOI: 10.3390/ma12091540

17. Lee, H., Kim, J.-H.J., Moon, J.-H., Kim, W.-W., Seo, E.-A. Evaluation of the Mechanical Properties of a 3D-Printed Mortar. Materials. 2019. 12 (24). 4104. DOI: 10.3390/ma12244104

18. Song, H., Li, X. An overview on the rheology, mechanical properties, durability, 3D printing, and microstructural performance of nanomaterials in cementitious composites. Materials. 2021. 14 (11). 2950. DOI: 10.3390/ma14112950

19. Albar, A., Chougan, M., Al- Kheetan, M.J., Swash, M.R., Ghaffar, S.H. Effective extrusion-based 3D printing system design for cementitious-based materials. Results in Engineering. 2020. 6. 100135. DOI: 10.1016/j.rineng.2020.100135

20. Wolfs, R.J.M., Bos, F.P., Salet, T.A.M. Hardened properties of 3D printed concrete: The influence of process parameters on interlayer adhesion. Cement and Concrete Research. 2019. 119. P. 132–140. DOI: 10.1016/j.cemconres.2019.02.017

21. Soltan, D.G., Li, V.C. A self-reinforced cementitious composite for building-scale 3D printing. Cement and Concrete Research. 2018. 90. Pp. 1–13. DOI: 10.1016/j.cemconcomp.2018.03.017

22. Perrot, A., Pierre, A., Nerella, V.N., Wolfs, R.J.M., Keita, E., Nair, S.A.O., Neithalath, N., Roussel, N., Mechtcherine, V. From analytical methods to numerical simulations: A process engineering toolbox for 3D concrete printing. Cement and Concrete Composites. 2021. 122. 104164. DOI: 10.1016/j.cemconcomp.2021.104164

23. Mechtcherine, V., Bos, F.P., Perrot, A., Leal da Silva, W.R., Nerella, V.N., Fataei, S., Wolfs, R.J.M., Sonebi, M., Roussel, N. Extrusion-based additive manufacturing with cement-based materials – Production steps, processes, and their underlying physics: A review. Cement and Concrete Research. 2020. 132. 106037. DOI: 10.1016/j.cemconres.2020.106037

24. Roussel, N., Bessaies-Bey, H., Kawashima, S., Marchon, D., Vasilic, K., Wolfs, R. Recent advances on yield stress and elasticity of fresh cement-based materials. Cement and Concrete Research. 2019. 124. 105798. DOI: 10.1016/j.cemconres.2019.105798

25. Slavcheva G.S., Artamonova O.V., Britvina E.A., Babenko D.S., Ibryayeva A.I. Dvukhfaznaya smes na osnove tsementa dlya kompozitov v tekhnologii stroitelnoy 3D-pechati [Two-phase mixture based on cement for composites in construction 3d printing technology]. Patent Russia No. 2729085, 2020.

26. Slavcheva G.S., Artamonova O.V., Britvina E.A., Babenko D.S., Ibryayeva A.I. Dvukhfaznaya smes na osnove tsementa dlya kompozitov v tekhnologii stroitelnoy 3D-pechati [Two-phase mixture based on cement for composites in construction 3d printing technology]. Patent Russia No. 2729283, 2020.

Contacts:

Galina Slavcheva, *Doctor of Technical Sciences*
ORCID: https://orcid.org/0000-0001-8800-2657
E-mail: gslavcheva@yandex.ru

Artem Levchenko, *PhD in Technical Sciences*
ORCID: https://orcid.org/0000-0002-6875-754X
E-mail: Alevchenko@vgasu.vrn.ru

Maria Shvedova,
ORCID: https://orcid.org/0000-0002-6484-8719
E-mail: marishwedowa@mail.ru

Davut Karakchi-ogly,
E-mail: karakchiogli.david@mail.ru

Dmitry Babenko,
E-mail: babenko.dmitrii@bk.ru